Elucidate the Formation Mechanism of Particulate Nitrate Based on Direct Radical Observations in the Yangtze River Delta summer 2019

Tianyu Zhai[a], *Keding Lu*[a, b*], *Haichao Wang*[c], *Shengrong Lou*[d], *Xiaorui Chen*[a, f], *Renzhi Hu*[e], *Yuanhang Zhang*[a, b*]

[a] State Key Joint Laboratory of Environmental Simulation and Pollution Control, College of Environmental Sciences and Engineering, Peking University, Beijing 100871, China.

[b] Collaborative Innovation Center of Atmospheric Environment and Equipment Technology, Nanjing University of Information Science & Technology, Nanjing 210044, China.

[c] School of Atmospheric Sciences, Sun Yat-sen University, Guangzhou 510275, China.

[d] State Environmental Protection Key Laboratory of Formation and Prevention of the Urban Air Complex, Shanghai Academy of Environmental Sciences, Shanghai, 200223, China.

[e] Key Laboratory of Environmental Optics and Technology, Anhui Institute of Optics and Fine Mechanics, Chinese Academy of Sciences, Hefei, 230031, China.

[f] Now at: Department of Civil and Environmental Engineering, The Hong Kong Polytechnic University, Hong Kong, China.

[*] *Correspondence to:*

Keding Lu (k.lu@pku.edu.cn), Yuanhang Zhang (yhzhang@pku.edu.cn)

Abstract. Particulate nitrate (NO_3^-) is one of the dominant components of fine particles in China, especially during pollution episodes, and has a significant impact on human health, air quality, and climate. Here a comprehensive field campaign that focuses on the atmospheric oxidation capacity and aerosol formation and their effects in the Yangtze River Delta (YRD) was conducted from May to June 2019 at a regional site in Changzhou, Jiangsu province in China. The concentration of NO_3^-, OH radical, N_2O_5, NO_2, O_3, and relevant parameters were measured simultaneously. We showed a high NO_3^- mass concentration with 10.6 ± 8.9 μg m^{-3} on average, which accounted for 38.3 % of total water-soluble particulate components and 32.0 % of total $PM_{2.5}$, followed by the proportion of sulfate, ammonium, and chloride by 26.0 %, 18.0 %, and 2.0 %, respectively. This result confirmed that the heavy nitrate pollution in eastern China not only happened in winter but also in the summertime. This study's high nitrate oxidation ratio (NOR) emphasized the solid atmospheric oxidation and fast nitrate formation capacity in YRD. It was found that OH + NO_2 during daytime dominated nitrate formation on clean days, while N_2O_5 hydrolysis vastly enhanced and became comparable with that of OH + NO_2 during polluted days (67.2 % and 30.2 %, respectively). An updated observed-constrain Empirical Kinetic Modeling Approach (EKMA) was used to assess the kinetic controlling factors of both local O_3 and NO_3^- productions, which indicated that the O_3-targeted scheme (VOCs: NO_x = 2: 1) is adequate to mitigate the O_3 and nitrate pollution coordinately during summertime in this region. Our results promote the understanding of nitrate pollution mechanisms and mitigation based on field observation and model simulation and call for more attention to nitrate pollution in the summertime.

Keywords:

Nitrate pollution; Dinitrogen pentoxide; Nitrate formation; Pollution mitigation

1 Introduction

Chemical compositions of fine particles have been measured in China during the past twenty years, and secondary inorganic aerosol is regarded as one of the dominant species in aerosol (Cao et al., 2012; Hagler et al., 2006; Zhao et al., 2013; Andreae et al., 2008). Since the Air Pollution Prevention and Control Action Plan, there has been a significant decrease in SO_2, NO_2, and $PM_{2.5}$ concentration in China, while the inorganic nitrate ratio in $PM_{2.5}$ increased and became the considerable component in $PM_{2.5}$ (Shang et al., 2021; Zhang et al., 2022). Therefore, a comprehensive understanding of the particlate nitrate formation mechanism is essential and critical to mitigating haze pollution in China.

Massive research has been done in China to investigate nitrate formation mechanisms, and a basic framework has been established (Sun et al., 2006; Chang et al., 2018; Wu et al., 2019). In the daytime, NO_2 + OH radical oxidation (Reaction 1) is the major particulate nitrate formation pathway. The product (HNO_3) reacts with alkaline substances in aerosol, generating particulate nitrate. This pathway is mainly controlled by precursors concentration as well as the gas-particle partition of gaseous nitric acid, and particulate nitrate depends on temperature, relative humidity (RH), NH_3 concentration, and aerosol acidity (Wang et al., 2009; Song and Carmichael, 2001; Meng et al., 2020; Zhang et al., 2021). At night, N_2O_5 uptake is a vital nitrate formation pathway (Reaction 4)(Chen et al., 2020; Wang et al., 2022). N_2O_5 is formed through $NO_2 + NO_3$ (Reaction 3) and there exists a quick thermal equilibrium balance (K_{eq} = 5.5 × 10^{-17} cm^{-3} $molecule^{-1}$ s^{-1}, 298 K). However, two problems remain ambiguous in quantifying the contribution of N_2O_5 uptake to nitrate formation. The first is the N_2O_5 heterogeneous uptake coefficient (γ) on ambient aerosol is highly varied with the range from 10^{-4} to 10^{-1} based on previous lab and field measurements (Bertram and Thornton, 2009; Brown et al., 2009; Wang et al., 2017c; Wang and Lu, 2016). The other one is $ClNO_2$ production yield which influences nitrate contribution due to the extensive variation range (Phillips et al., 2016; Staudt et al., 2019; Tham et al., 2018). Both two

parameters are complex to well-predicted by current schemes. NO_2 heterogeneous uptake has been found nonnegligible for nitrate formation, which can be a vital pathway during heavy haze events, according to recent studies (Qiu et al., 2019; Chan et al., 2021). The uptake coefficient and nitrate yield remain uncertain, as same as the N_2O_5 heterogeneous reaction. Besides, N_2O_5 homogeneous hydrolysis and NO_3 radical oxidation have a minor contribution to particulate nitrate under ambient conditions(Brown et al., 2009; Seinfeld and Pandis, 2016).

$$NO_2 + OH \rightarrow HNO_3 \quad \text{R1}$$

$$NO_2 + O_3 \rightarrow NO_3 + O_2 \quad \text{R2}$$

$$NO_2 + NO_3 + M \rightarrow N_2O_5 + M \quad \text{R3.1}$$

$$N_2O_5 + M \rightarrow NO_2 + NO_3 + M \quad \text{R3.2}$$

$$N_2O_5 + (H_2O \text{ or } Cl^-) \rightarrow (2 - \varphi)\, NO_3^- + \varphi ClNO_2 \quad \text{R4}$$

As a critical area of China's economy and industry, Yangtze River Delta (YRD) has suffered severe air pollution during past decades, and fine particle pollution in YRD has raised a widespread concern (Guo et al., 2014; Zhang et al., 2015; Zhang et al., 2017; Ming et al., 2017; Xue et al., 2019). However, most research focuses on wintertime $PM_{2.5}$ pollution and lacks measurements of critical intermediate species and radicals to assess the importance of each nitrate formation pathway. In this study, with the direct measurements of hydroxyl radical and the reactive nitrogen compounds and chemical box model analysis, we explore the characteristics of nitrate and precursors in YRD in the summer of 2019, the importance of particulate nitrate formation pathways is quantified, and the controlling factors are explored. A further suggestion for summer pollution prevention and control in the local area is proposed.

2 Site description and methods

2.1 The campaign site

This campaign took place at a suburban sanatorium from May 30th to June 18th, 2019, in Changzhou, China. Changzhou (119.95 °E, 31.79 °N) is located in Jiangsu province and about 150 km northwest of Shanghai. The sanatorium, located 420 m east of Lake Ge (one of the largest lakes in Jiangsu province, 164 square kilometers), is surrounded by farmland and fishponds. With the closest arterial traffic 1 km away, several industry zones are 4 km to the east. The prevailing wind was from the south and southeast sectors (about 30 % of the time) compared to 20 % from the west sector, of which only 15 % came from the east. The wind speed was usually lower than 5 m s^{-1} with faster speed from the west. This site was influenced by anthropogenic and biological sources with occasional biomass burning.

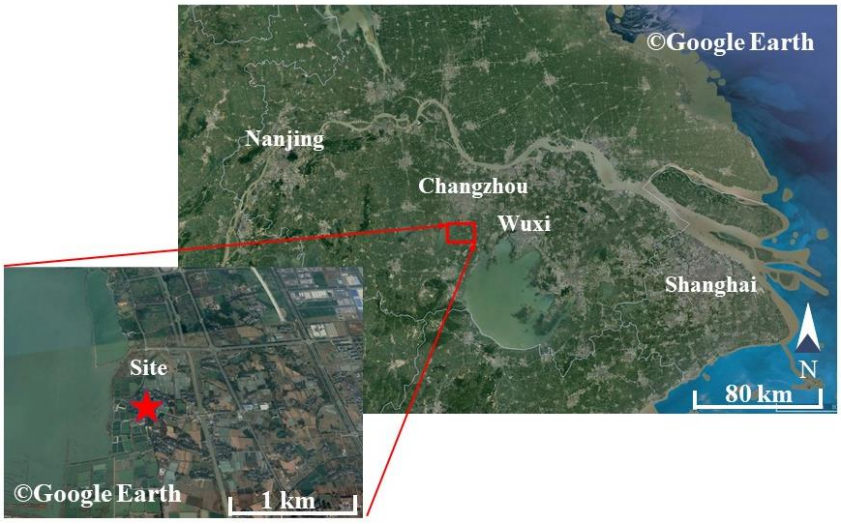

Figure 1 The location of the campaign site (red star), Changzhou, is 150 km on the northwest side of Shanghai.

2.2 The instrumentation

Multiple gaseous and particlate parameters were measured simultaneously during the

campaign to comprehensively interpret the nocturnal atmospheric capacity and aerosol formation. The related instruments are listed in Table 1. N_2O_5 and Particle Number and Size Distribution (PNSD) were measured on the fourth floor of the sanatorium, which is the top of the building. Other instruments were placed in containers on the ground 170 m northeast of the building, and sampling inlets at circa 5 m above the ground through the containers' roof.

N_2O_5 was measured by Cavity Enhanced Absorption Spectrometer (CEAS) based on Lambert-Beer's law which was developed by (Wang et al., 2017b). Briefly, air samples were drawn through the window and reached out of the wall 30 cm to prevent influence from surface deposition. The aerosol membrane filter was deployed before the PFA sampling tube and changed every 2 hours at night to avoid a decrease in N_2O_5 transmission efficiency due to the increased loss of N_2O_5 from the accumulated aerosols on the filter. N_2O_5 was decomposed to NO_3 and NO_2 through preheating tube heat at 130 ℃ and detected within a PFA-coated resonator cavity heated at 110 ℃ to prevent the formation of N_2O_5 by reversible reaction subsequently. At the end of each sampling cycle (5 min), a 30 s injection of high concentration NO (10 ppm, 20 ml min^{-1}) mixed with sample air was set to eliminate NO_3-N_2O_5 in the system. The NO titration spectrums were adopted as the dynamic background spectrum by assuming no H_2O concentration variation in a single sampling cycle. The loss of N_2O_5 in the sampling system and filter was also considered during data correction. The limit of detection (LOD) was estimated to be 2.7 pptv (1 σ) with an uncertainty of 19 %.

OH radical measurement was conducted by Fluorescence Assay by Gas Expansion Laser-Induced Fluorescence techniques (FAGE-LIF). Ambient air was expanded through a 0.4 mm nozzle to low pressure in a detection chamber, where the 308 nm laser pulse irradiated OH radical at a repetition rate of 8.5 kHz (Chen et al., 2018). NO_x and O_3 were monitored by commercial monitors (Thermo-Fisher 42i and 49i). Volatile organic compounds (VOCs) were measured by an automated Gas Chromatograph equipped with a Mass Spectrometer and flame ionization detector (GC-MS) with a time

resolution of 60 min. The photolysis frequencies were determined from the spectral actinic photon flux density measured by a spectroradiometer (Bohn et al., 2008).

$PM_{2.5}$ concentration was obtained by Tapered Element Oscillating Microbalance (TEOM 1405, Thermo Scientific Inc). Aerosol surface concentration (S_a) was converted from particle number and size distribution, which was measured by Scanning Mobility Particle Sizer (SMPS, TSI 3936) and Aerosol Particle Sizer (APS, TSI 3321) and modified to the wet particle-state S_a with a hygroscopic growth factor (Liu et al., 2013). The uncertainty of the wet S_a was ~ 30 %. Meanwhile, water-soluble particulate components and their gaseous precursors were analyzed through the Monitor for AeRosols and GAses in ambient air (MARGA, Chen et al. (2017)). Meteorological data were also available, including the temperature, relative humidity (RH), pressure, wind speed, and wind direction.

Table 1 The observed gas and particle parameters during the campaign.

Parameters	Detection of limit	Method	Accuracy
N_2O_5	2.7 pptv (1 σ, 1 min)	CEAS	± 19 %
OH	1.6×10^5 cm^{-3} (1 σ, 60 s)	LIF[a]	± 21 %
NO	60 pptv (2 σ, 1 min)	PC[c]	± 10 %
NO_2	0.3 ppbv (2 σ, 1 min)	PC[c]	± 10 %
O_3	0.5 ppbv (2 σ, 1 min)	UV photometry	± 5 %
VOCs	20-300 pptv (60 min)	GC-MS	± 15 %
$PM_{2.5}$	0.1 μg m^{-3} (1 min)	TEOM[d]	± 5 %
Photolysis frequencies	5×10^{-5} s^{-1} (1 min)	SR[e]	± 10 %
PNSD	14 nm -700 nm (4 min)	SMPS, APS	± 10 %
HNO_3, NO_3, HCl	0.06 ppbv (30 min)	MARGA[f]	± 20 %
NH_4^+, NO_3^-, Cl^-, SO_4^{2-}	0.05 μg m^{-3} (30 min)	MARGA[f]	± 20 %

[a] Laser-induced fluorescence; [b] Chemiluminescence; [c] Photolytic converter; [d] Tapered Element Oscillating Microbalance; [e] Spectroradiometer; [f] the Monitor for AeRosols and GAses in ambient air.

2.3 The empirical kinetic modeling approach

A box model coupled with the Regional Atmospheric Chemical Mechanism version 2 (RACM2, Goliff, Stockwell & Lawson, 2013) is used to conduct the mitigation strategies studies. The model is operated in one-hour time resolution with measurement

results of temperature, relative humidity, pressure, CO, NO_2, H_2O, photolysis frequencies, and aggregated VOCs input to constrain the model. It should be noted that HONO concentration is calculated by NO_2 times 0.02, as suggested by Elshorbany et al. (2012), and has been used in the box model before (Lou et al., 2022). Long-lived species such as H_2 and CH_4 are assumed as constants (550 ppbv and 1900 ppbv, respectively). Moreover, a 13-hour constant loss rate of unconstrained intermediate and secondary products, the result of synthetic evaluating secondary simulation of secondary species, is set for representing the multi-effects of deposition, transformation, and transportation.

The approaches to the chemical production of O_3 ($P(O_3)$) and inorganic nitrate ($P(NO_3^-)$) are described in previous articles (Tan et al., 2021; Tan et al., 2018) and expressed as Equation 1 and 4:

$$P(O_3) = F(O_3) - D(O_3) \quad \text{Eq1}$$

$$F(O_3) = k_{HO_2+NO}[NO][HO_2] + k_{(RO_2+NO)eff}[NO][RO_2] \quad \text{Eq2}$$

$$D(O_3) = k_{OH+NO_2}[OH][NO_2] + (k_{OH+O_3}[OH] + k_{HO_2+O_3}[HO_2] + k_{alkenes+O_3}[alkenes])[O_3] \quad \text{Eq3}$$

$$P(NO_3^-) = P(HNO_3) + P(pNO_3^-) \quad \text{Eq4}$$

$$P(HNO_3) = k_{OH+NO_2}[OH][NO_2] \quad \text{Eq5}$$

$$P(pNO_3^-) = 0.25(2 - \varphi)\, C\, \gamma\, S_a\, [N_2O_5] \quad \text{Eq6}$$

briefly, $P(O_3)$ is net ozone production, which is calculated by peroxyl radial + NO oxidation (Eq. 2) minus the chemical loss of O_3 and NO_2 (Eq. 3). $P(NO_3^-)$ is constituted by reaction OH + NO_2 (Eq. 5) and N_2O_5 heterogeneous uptake (Eq. 6). Here, rate constants of reactions are obtained from NASA JPL Publication or RACM2 (Goliff et al., 2013). γ is the N_2O_5 uptake coefficient calculated from parameterization (γ_P, more details in chapter 3.3). φ represents $ClNO_2$ production yield through N_2O_5 hydrolysis, and the mean value reported by Xia et al. (2020) is used in this work.

The empirical Kinetic Modeling Approach (EKMA) was innovated to study the effects of precursors (VOCs and NO_x) reactivity on the region's ozone pollution by Kanaya et al., which helps recognize the region's susceptibility to precursors by weight and become a prevalent tool to study the process of ozone formation (Tan et al., 2018; Yu et al., 2020b; Kanaya et al., 2008). The prevention and control problem of pollutant generation can be transformed through the EKMA curve to reduce its precursors' emissions. Furthermore, the precursor reduction scheme needed for total pollutant control is given qualitatively. $P(NO_3^-)$ can also be analyzed through EKMA for the nonlinear secondary formation relationship with precursor reactivity. Here, an isopleth

diagram of the net ozone production rate as functions of the reactivities of NO_x and VOCs can be derived from EKMA. In detail, 0.01 to 1.2 emission reduction strategy assumptions are exponential interpolation into 20 kinds of emission situations of NO_x and VOCs, respectively, which counts 400 scenarios.

2.4 The calculation of aerosol liquid water content

Aerosol liquid water content (ALWC) is calculated through ISORROPIA II (Fountoukis and Nenes, 2007). Forward mode is applied in this study. Furthermore, water-soluble particulate components in $PM_{2.5}$ and gaseous species (NH_3 + HNO_3 + HCl) obtained from MARGA, along with RH and T, are input as initial input. In addition, metastable aerosol state is chosen due to high RH during this campaign.

3 Result and discussion

3.1 Overview of measurements

The time used in this study is China Standard Time (UTC + 8) and the local sunrise and sunset time during the campaign were around 5 am and 7 pm, respectively. The whole campaign period is divided into four $PM_{2.5}$ clean periods and four $PM_{2.5}$ polluted periods (9 out of 14 days, the latter polluted periods days day refer to $PM_{2.5}$ pollution except specified description) according to the Chinese National Air Quality Standard (CNAAQS) Grade I of daily $PM_{2.5}$ concentrations (< 35.0 μg m^{-3}). Figure 2 shows the meteorological parameters and gas-phase and particulate species timeseries during the observation. During the campaign, the temperature was high; the maximum reached 34.5 ℃, with an average of 25.1 ± 3.7 ℃. RH changed drastically from 21 % to 88 %, with a mean value of 58.9 ± 14.0 %. The mean NO_2 concentration was 14.8 ± 9.5 ppbv. Meanwhile, the O_3 average was 54.6 ± 28.8 ppbv, exceeding CNAAQS Grade II for a maximum daily average of 8 h ozone (160 μg m^{-3}) on 14 out of 19 days and exceeding 200 μg m^{-3} on six days.

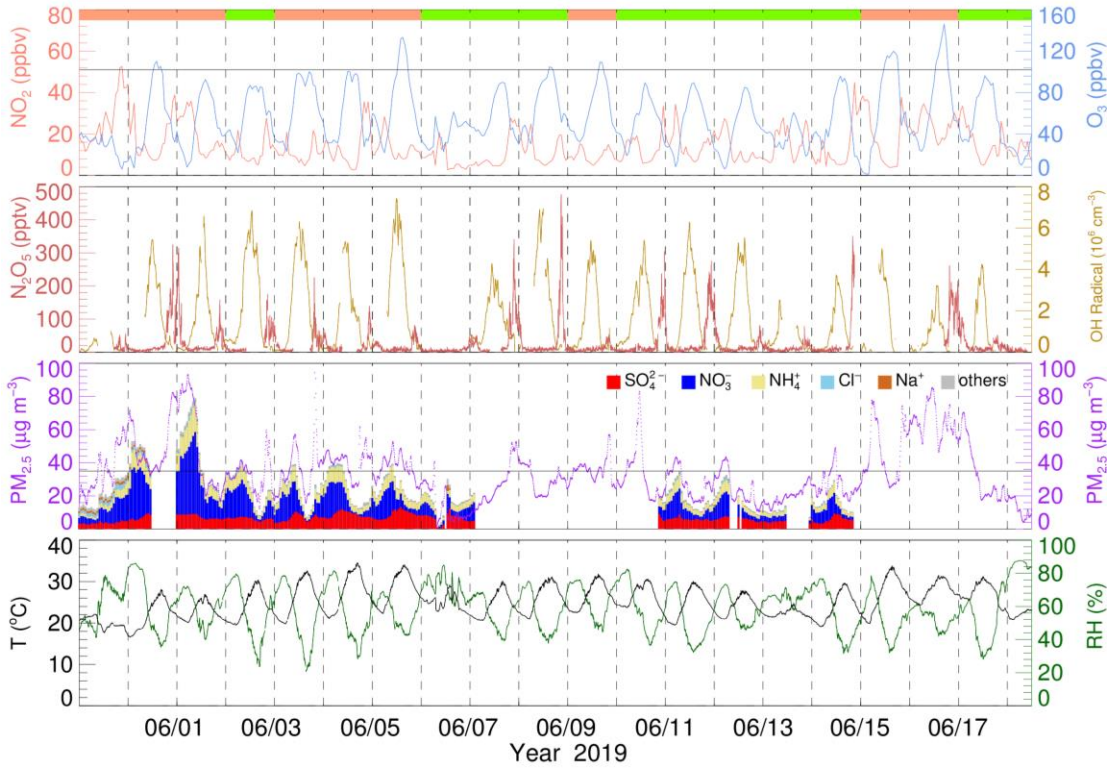

Figure 2 Timeseries of NO_2, O_3, N_2O_5, OH radical, $PM_{2.5}$, and water-soluble particulate components, temperature, and RH. The vertical dotted line represents the zero clock. The black horizontal solid line in O_3 and $PM_{2.5}$ panels represents Chinese national air quality standards for O_3 and $PM_{2.5}$, respectively. The top panel color blocks represent the $PM_{2.5}$ clean day (light green) and $PM_{2.5}$ polluted day(salmon).

Daytime OH radical ranged from 2×10^6 to 8×10^6 molecular cm^{-3} with a daily peak over 3×10^6 molecular cm^{-3}. Maximum OH radical reached 8.18×10^6 molecular cm^{-3} in this campaign. Compared with other summertime OH radical observed in China, OH radical concentration in this site is relatively low but still on the same order of magnitude (Lu et al., 2012; Lu et al., 2013; Ma et al., 2022; Tan et al., 2017; Woodward-Massey et al., 2020; Yang et al., 2021). N_2O_5 mean concentration was 21.9 ± 39.8 pptv with a nocturnal average of 61.0 ± 63.1 pptv and a daily maximum of over 200 pptv at eight nights. The maximum concentration of N_2O_5 (477.2 pptv, 5 min resolution) appeared at 20:47 on June 8th. The average NO_3 radical production rate $P(NO_3)$ is 2.1 ± 1.4 ppbv h^{-1} with nocturnal average $P(NO_3)$ 2.8 ± 1.6 ppbv h^{-1} and daytime $P(NO_3)$ 2.2 ± 1.4 ppbv h^{-1}. $P(NO_3)$ is about twice of documented value in Taizhou and North China Plain (Wang et al., 2017a; Wang et al., 2018b; Wang et al., 2020a), but close to

another result in YRD before (Chen et al., 2019). The average $PM_{2.5}$ was 34.6 ± 17.8 μg m^{-3} with a maximum reach of 163.0 μg m^{-3}. The water-soluble particulate components of $PM_{2.5}$ are displayed as well. The average NO_3^- concentration was 10.6 μg m^{-3}, which accounts for 38.3 % mass concentration of water-soluble particulate components and 32.0 % total $PM_{2.5}$, while the proportion of sulfate, ammonium, and chloride is 26.0 %, 18 %, and 2.0 % respectively. To sum up, during the campaign period, the pollution of $PM_{2.5}$ would be generally exacerbated on high O_3 and NO_2 days. Precipitation occurred during four clean processes receded pollutant concentration; otherwise, the pollution condition remained severe.

The mean diurnal variations (MDC) of temperature, RH, NO_2, O_3, $P(NO_3)$, N_2O_5, OH radical, and $PM_{2.5}$ in different air quality are shown in Figure 3. The temperature, RH, and OH radical MDC show indistinctive differences between clean days (CD) and polluted days (PD). The MDC of NO_2 has two concentration peaks that appear at 06:00 and 21:00 on CD, while at PD, its peak appears at 20:00 and maintains a high level during the whole night. O_3 diurnal pattern reflects a typical urban-influenced character with a maximum O_3 peak that lasts four hours from 14:00 to 17:00, while polluted-day O_3 peak concentration is 1.2 higher than clean-day. $P(NO_3)$ grows after the O_3 peak and maximum $P(NO_3)$ shows at 19:00 with an average value of 1.7 ppbv h^{-1} on CD. By contrast, the mean polluted-day P(NO3) is 2.6 ppbv h-1, and the maximum value reaches 4.7 ppbv h^{-1}. In contrast, the clean-day N_2O_5 has a higher average and maximum concentration than PD, which suggests a faster removal process during PD. $PM_{2.5}$ has a similar trend with $P(NO_3)$ and has a higher concentration during nighttime.

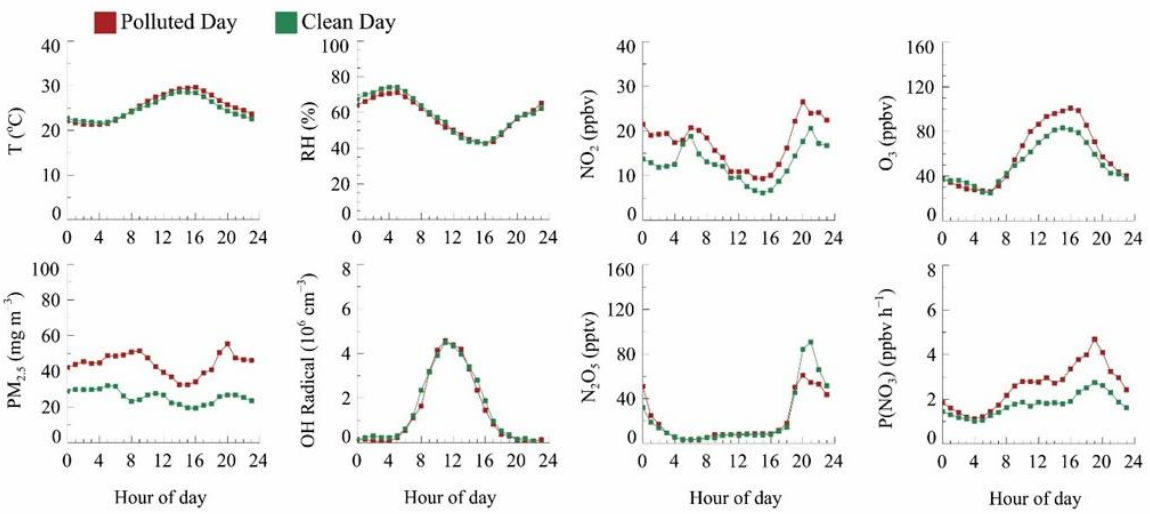

Figure 3 The mean diurnal variations of temperature, RH, NO_2, O_3, $PM_{2.5}$, OH radical(orange), N_2O_5, and $P(NO_3)$ of clean day and polluted day.

3.2 The evolution of nitrate pollution

Figure 4 (a) shows the relationship between nitrate and sulfate with water-soluble particulate components. Nitrate positively correlates with total water-soluble particulate components, while the sulfate ratio has an inverse correlation. With $PM_{2.5}$ concentration increasing, nitrate proportion increases rapidly and keeps high weight at heavy $PM_{2.5}$ period while sulfate ratio pears opposite phenomenon. Once the mass concentration of total water-soluble particulate component is over 30 μg m^{-3}, the mass fraction of nitrate in total water-soluble particulate components is up to 50 % on average. This result illustrates that particulate nitrate is one of the vital sources of explosive growth particulate matter.

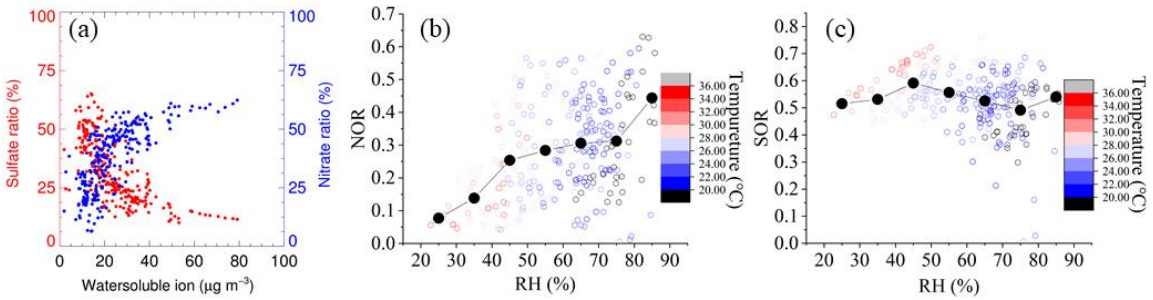

Figure 4 (a) Particulate ion mass concentration ratio of nitrate and sulfate to water-soluble ion. (b) NOR against RH, colored with temperature. (c) SOR against RH, colored with temperature.

To further assess the conversion capacity of nitrate and sulfate in this site, the sulfur oxidation ratio (SOR) and the nitrogen oxidation ratio (NOR) are used to indicate the secondary transformation ratio of SO_2 and NO_2, respectively (Sun et al., 2006). SOR and NOR are estimated using the formulae below:

$$SOR = \frac{nSO_4^{2-}}{nSO_4^{2-}+nSO_2} \quad \text{Eq7}$$

$$NOR = \frac{nNO_3^-}{nNO_3^-+nNO_2} \quad \text{Eq8}$$

Where n refers to the molar concentration, the higher SOR and NOR represent more oxidation of gaseous species into a secondary aerosol. As depicted in Figure 4 (b-c), NOR rapidly increases at RH < 45 %, remains constant at 45 % < RH < 75 %, and ends with a sharp increase at RH > 75 %. During the study period, not only is the average concentration of NO2 higher among PD but there is also a significant difference between PD and CD NOR. The average values of NOR are 0.32 in PD and 0.25 in CD, respectively, which manifests the more secondary transformation and pollution potential in PD. In contrast, the SOR stays constant at a high value (~ 0.5) during the whole RH scale, which shows a different pattern from previous research (Li et al., 2017; Zheng et al., 2015). One possible explanation is that SO_2 concentration stays low during the whole campaign (4.4 ± 2.4 ppbv on average), and SO_2 oxidation depends on the limit of SO_2 instead of oxidation capability. Meanwhile, the mean SOR in both situations is over 0.5 (0.52 in CD and 0.56 in PD), further supporting the SO_2 limited hypothesis. Besides, Table 2 summarizes NOR and SOR values in YRD. NOR and SOR in this study are similar to values reported in other YRD research (Shu et al., 2019; Zhang et al., 2020b; Qin et al., 2021; Zhao et al., 2022), except values in 2013 , but higher than north China study which emphasize the solid atmospheric oxidation capacity in YRD region.

Table 2 Statistical result of NOR and SOR in YRD

Location and Year	SOR				NOR				References
	Max	Min	Mean	SD	Max	Min	Mean	SD	
Nanjing 2013 Winter	0.42	0.10	0.28	0.11	0.29	0.15	0.21	0.05	
Suzhou 2013 Winter	0.41	0.15	0.27	0.11	0.30	0.06	0.16	0.08	
Lin'an 2013 Winter	0.50	0.19	0.35	0.11	0.24	0.12	0.18	0.05	
Hangzhou 2013 Winter	0.30	0.14	0.21	0.06	0.11	0.06	0.09	0.02	
Ningbo 2013 Winter	0.35	0.09	0.21	0.11	0.23	0.03	0.11	0.07	
YRD 2016 Summer	-	-	0.347	-	-	-	0.11	-	
YRD 2016 Winter	-	-	0.247	-	-	-	0.15	-	
Nanjing 2019 spring	0.48	0.38	-	-	0.31	0.29	-	-	
Changzhou 2019 spring	0.35	0.3	-	-	0.27	0.23	-	-	
Changzhou 2019 Winter	0. 68	0.24	0.35	0.12	0.44	0.13	0.2	0.1	
Changzhou 2019 Summer	0.16	0.76	0.54	0.1	0.08	0.63	0.28	0.14	This work

3.3 The derivation of N_2O_5 uptake coefficient

Statistical analysis of the observation above highlights the rapid formation of particulate nitrate. To assess the contribution of N_2O_5 hydrolysis to particular nitrate formation, two methods are applied to calculate the N_2O_5 uptake coefficient. The first method is a stationary-state approximation (Brown et al., 2003). By assuming that the rates of production and loss of N_2O_5 are approximately in balance, the total loss rate of N_2O_5 ($k_{N_2O_5}$) can be calculated through equation 9. The $k_{N_2O_5}$ is main dominated by N_2O_5 heterogeneous uptake, since homogeneous hydrolysis of N_2O_5 contribute tiny (Brown and Stutz, 2012). N_2O_5 uptake coefficient through steady-state (note as γ_S) is derived as equation 10. Here C is the mean molecule speed of N_2O_5, and S_a is the aerosol surface concentration.

$$\tau_{ss}(N_2O_5) = \frac{[N_2O_5]}{k_{R3.1}[NO_2][O_3]} = \left(k_{N_2O_5} + \frac{k_{NO_3}}{K_{eq}[NO_2]}\right)^{-1} \quad \text{Eq9}$$

$$k_{N_2O_5} = 0.25\, C\, \gamma_S\, S_a \quad \text{Eq10}$$

Due to the fast variety of NO_3 loss rates from VOCs, the steady-state method has been unattainable in conditions affected by emission interferences. During the whole campaign, we only retrieve three valid fitting results. As shown in Figure 5, the fitted

$\gamma_{\_S}$ ranged from 0.057 to 0.123, which is comparable with Taizhou (0.041, Wang et al. (2020a)) and much higher than other results in China (Yu et al., 2020a; Wang et al., 2018a; Wang et al., 2020b; Wang et al., 2017a). The calculated k_{NO_3} ranged from 0.002 to 0.16 s^{-1}, represents drastic VOCs change during this campaign.

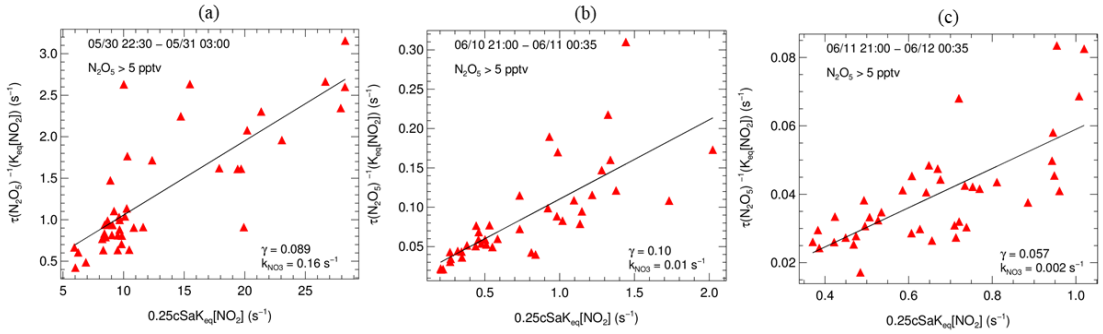

Figure 5 Derived N_2O_5 uptake coefficients from N_2O_5 steady lifetime ($\gamma_{\_S}$) with NO_2 and S_a, plots (a-c) represent the linear fitting results on the nights of 05/30, 06/10, and 06/11, respectively.

The other approach is the parameterization by (Yu et al., 2020a) which is depicted as follows:

$$\gamma_{\_P} = \frac{4}{c}\frac{V_a}{S_a} K_H \times 3.0 \times 10^4 \times [H_2O] \left(1 - \frac{1}{\left(0.033 \times \frac{[H_2O]}{[NO_3^-]}\right) + 1 + \left(3.4 \times \frac{[Cl^-]}{[NO_3^-]}\right)}\right) \quad \text{Eq11}$$

Where V_a/S_a is the measured aerosol volume to surface area ratio by SMPS; K_H is Henry's law coefficient which is set as 51 as recommended; $[NO_3^-]$ and $[Cl^-]$ are aerosol inorganic concentration measured by Marga; $[H_2O]$ is aerosol water content calculated through ISORROPIA II. The valid parameterization calculated N_2O_5 uptake coefficient (note as $\gamma_{\_P}$) from May 30th to June 08th, 2019, shows in Figure 6 a good consistency between the trends of $\gamma_{\_P}$ and aerosol water content. Nighttime $\gamma_{\_P}$ varies from 0.001 to 0.024 with an average of 0.069 ± 0.0050 in polluted condition and 0.0036 ± 0.0026 in clean condition. The N_2O_5 uptake coefficient shows a good correlation between RH and aerosol water content. For the N_2O_5 uptake coefficient, although particulate nitrate mass concentration increased during the pollution event, an antagonistic effect on the N_2O_5 uptake coefficient was not obvious for the nitrate molarity decreasing.

Furthermore, we compare the difference between $\gamma_{\_S}$ and $\gamma_{\_P}$ [h]. Taking the night of May 30th as an example, the $\gamma_{\_S}$ is 0.089 while $\gamma_{\_P}$ ranges from 0.024 to 0.057 with an average value of 0.013 ± 0.0051. The difference between steady-state and parameterization is significant; one possible explanation is uncertainty for stationary-state approximation caused by local NO or VOCs emission (Brown et al., 2009; Chen et al., 2022). Another reason is that parameterization by Yu et al. ignores the impact of organic matter on the fine particle. The difference in aerosol composition between this work and Yu et al may also bring uncertainty. Overall consideration, $\gamma_{\_P}$ will be chosen for the N_2O_5 heterogeneous uptake coefficient in later analysis and discussion.

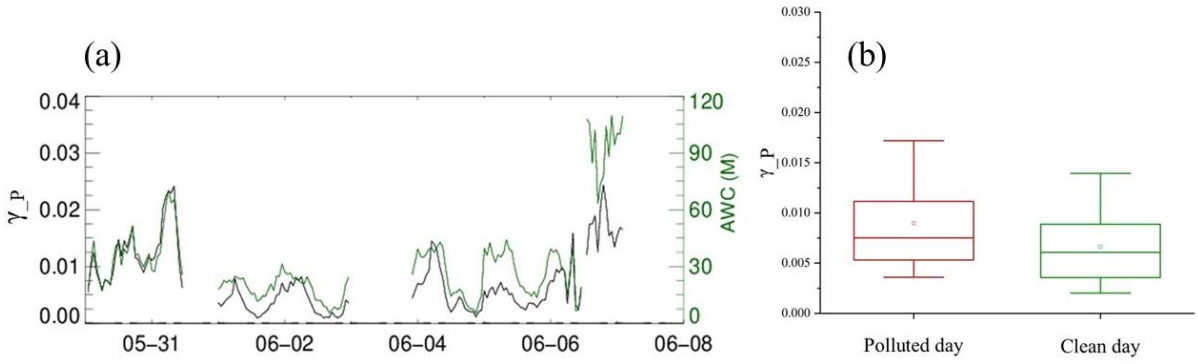

Figure 6 Results of N_2O_5 uptake coefficients through parameterization ($\gamma_{\_p}$). (a) shows timeseries of $\gamma_{\_p}$ and ISORROPIA II results of aerosol water content (AWC). (b) is the box-plot of $\gamma_{\_p}$ on the polluted day and clean day, the hollow square represents the mean value, and the solid line across the box shows the median score for the data set, while the top and bottom whiskers represent 90 % and 10 % value of $\gamma_{\_p}$, respectively.

3.4 Quantifying the contribution of nitrate formation pathways

After the N_2O_5 uptake coefficient is counted, nitrate production potential ($P(NO_3^-)$) can be calculated. Here N_2O_5 uptake coefficient is set as 0.036 on clean day and 0.069 on polluted day, respectively, which are the average value derived from parameterization. The production ratio of NO_3^- (by considering $ClNO_2$ yield of 0.54) is set as 1.46 in the former study (Xia et al., 2020). Gas particle distribution is considered by the result of particular nitrate and gas-phase nitrate by MARGA (input HNO_3/NO_3^- ratio to the model as OH + NO_2 nitrate production rate). NO_2 heterogeneous uptake coefficient is set

as 5.8×10^{-6} depending on the report by Yu et al. (2021) which is the result of 70% RH on urban grime.

The mean diurnal variations of the nitrate production potential of clean and polluted day are depicted in Figure 7. The OH + NO_2 pathway shows no significate difference between clean and polluted day and dominates clean day nitrate formation potential. Since the level of OH and NO_2 is less affected by the fine particle level. However, the rapid increase of the N_2O_5 heterogeneous uptake pathway on polluted day is fatal, and its peak formation rate at night over the OH + NO_2 pathway can be used to explain nighttime nitrate explosive growth.

As shown in Figure 7c, OH + NO_2 dominates nitrate production on clean day, while the N_2O_5 uptake pathway only contributes 13.6 μg m^{-3}. On polluted days, the ability of N_2O_5 uptake grows fast, reaching 50.1 μg m-3, while the OH pathway doesn't change much. There is no distinct difference in the daytime pathway (OH + NO_2) between clean day and polluted day, while the nighttime pathway ratio rises from 38.1 % on clean day to 67.2 % on polluted day.NO_2 heterogeneous uptake increases from 0.93 μg m^{-3} on clean day to 2.0 μg m^{-3} on polluted day, but the contribution proportion does not change obviously. Both the higher N_2O_5 uptake coefficient and higher S_a on polluted day increase the contribution of N_2O_5 hydrolysis on particular nitrate at pollution condition.

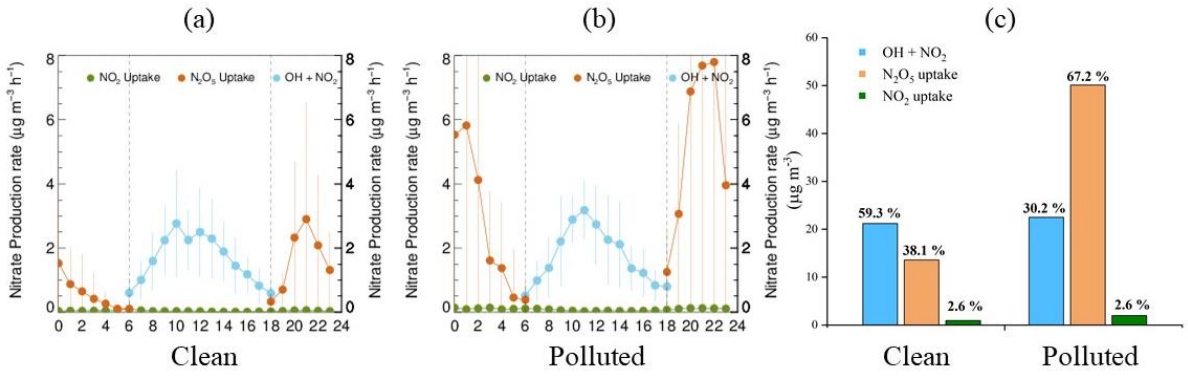

Figure 7 The mean diurnal variations of the nitrate production potential of clean day(a) and polluted day (b) and the P(NO_3^-) distribution of clean and polluted day (c).

3.5 Mitigation strategies of particulate nitrate and ozone productions

We selected two pollution episodes (Episode I (2019.05.30 00:00 - 2019.06.02 00:00) and IV (2019.06.14 17:30 - 2019.06.17 12:00)) to explore the mitigation way of ozone and nitrate pollution. Figure 8 shows the EKMA of $P(O_3)$ and $P(NO_3^-)$ of these two periods, O_3 located at VOCs controlling area in the two pollution episodes, which consist with previous YRD urban ozone sensitivity study (Jiang et al., 2018; Zhang et al., 2020a; Xu et al., 2021). The best precursor reduction for O_3 is VOCs: NO_x = 2:1 while nitrate is located at the transition area, which means either of the precursors reduction will mitigate nitrate pollution. For the regional and complex air pollution characteristics in this region, a fine particle-targeting reduction scheme will aggravate O_3 pollution. In contrast, the O_3-targeting scheme can mitigate O_3 and fine particle simultaneously.

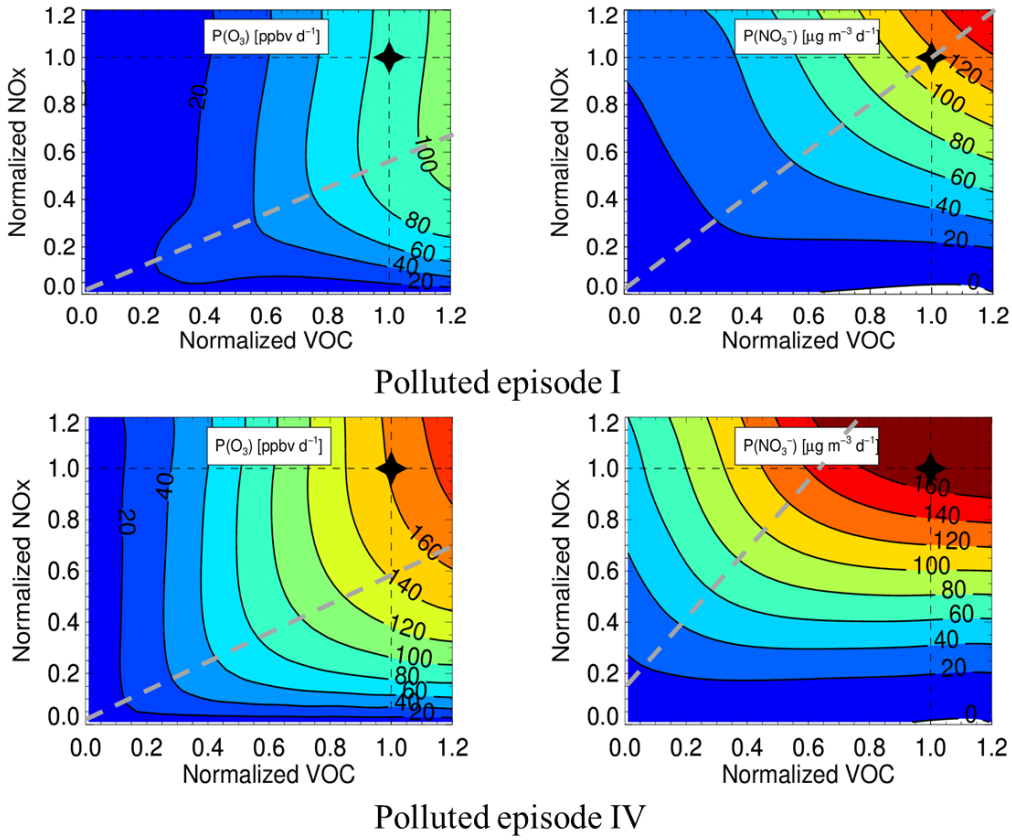

Figure 8 Isogram of $P(O_3)$ and $P(NO_3^-)$ of polluted episode I (2019.05.30 00:00 - 2019.06.02 00:00) and IV (2019.06.14 17:30 - 2019.06.17 12:00) with different NOx and VOC reduction degree. The grey dash line represents the ridge line.

4 Conclusion

A comprehensive campaign was conducted to interpret the atmospheric oxidation capacity and aerosol formation from May 30th to June 18th, 2019, in Changzhou, China. The high O_3 and $PM_{2.5}$ concentrations confirm complex air pollution characteristics in Changzhou, and nitrate accounts for 38.3 % mass concentration of total water-soluble particulate components and 32.0 % of total $PM_{2.5}$. In addition, the average values of NOR are 0.32 in PD and 0.25 in CD. The positive correlation between NOR and RH and inverse correlation refer to the contribution of N_2O_5 heterogeneous uptake to nitrate formation.

Based on field observations of OH and related parameters, we show OH oxidation of the NO_2 pathway steadily contributes to nitrate formation no matter the clean or polluted period and domination clean day nitrate production (about 22 μg m^{-3}). N_2O_5 heterogeneous uptake contribution proliferated on polluted day, from 13.6 μg m^{-3} (38.1 %) on clean days to 50.1 μg m^{-3} (67.2 %) on polluted days. NO_2 heterogeneous uptake contributes minor to nitrate formation (2.6 %).

The precursor reduction simulation suggests the reduction ratio of VOCs: NO_x equals 2:1 can simultaneously and effectively mitigate O_3 and fine particle pollution during the summertime complex pollution period in Changzhou. To more precisely and delicately establish a cooperative control scheme for regional O_3 and nitrate, the regional and long-time field campaigns are needed in the future to analyze the seasonal and interannual variation of O_3 and nitrate and relevant parameters.

Code/Data availability. The datasets used in this study are available from the corresponding author upon request (k.lu@pku.edu.cn).

Author contributions. K.D.L. and Y.H.Z. designed the study. T.Y.Z analyzed the data and wrote the paper with input from all authors.

Competing interests. The authors declare that they have no conflicts of interest.

Acknowledgments. This project is supported by the National Natural Science Foundation of China (21976006); the Beijing Municipal Natural Science Foundation for Distinguished Young Scholars (JQ19031); the National Research Program for Key Issue in Air Pollution Control (DQGG0103-01, 2019YFC0214800). Thanks for the data contributed by field campaign team.

References

Andreae, M. O., Schmid, O., Yang, H., Chand, D., Yu, J. Z., Zeng, L.-M., and Zhang, Y.-H.: Optical properties and chemical composition of the atmospheric aerosol in urban Guangzhou, China, Atmospheric Environment, 42, 6335-6350, 10.1016/j.atmosenv.2008.01.030, 2008.

Bertram, T. H. and Thornton, J. A.: Toward a general parameterization of N2O5 reactivity on aqueous particles: the competing effects of particle liquid water, nitrate and chloride, Atmospheric Chemistry and Physics, 9, 8351-8363, 10.5194/acp-9-8351-2009, 2009.

Bohn, B., Corlett, G. K., Gillmann, M., Sanghavi, S., Stange, G., Tensing, E., Vrekoussis, M., Bloss, W. J., Clapp, L. J., Kortner, M., Dorn, H. P., Monks, P. S., Platt, U., Plass-Dülmer, C., Mihalopoulos, N., Heard, D. E., Clemitshaw, K. C., Meixner, F. X., Prevot, A. S. H., and Schmitt, R.: Photolysis frequency measurement techniques: results of a comparison within the ACCENT project, ACP, 8, 5373-5391, 10.5194/acp-8-5373-2008, 2008.

Brown, S. S. and Stutz, J.: Nighttime radical observations and chemistry, Chemical Society Reviews, 41, 6405-6447, 10.1039/c2cs35181a, 2012.

Brown, S. S., Stark, H., and Ravishankara, A. R.: Applicability of the steady state approximation to the interpretation of atmospheric observations of NO3 and N2O5, Journal of Geophysical Research-Atmospheres, 108, 10, 10.1029/2003jd003407, 2003.

Brown, S. S., Dube, W. P., Fuchs, H., Ryerson, T. B., Wollny, A. G., Brock, C. A., Bahreini, R., Middlebrook, A. M., Neuman, J. A., Atlas, E., Roberts, J. M., Osthoff, H. D., Trainer, M., Fehsenfeld, F. C., and Ravishankara, A. R.: Reactive uptake coefficients for N2O5 determined from aircraft measurements during the Second Texas Air Quality Study: Comparison to current model parameterizations, Journal of Geophysical Research-Atmospheres, 114, 10.1029/2008jd011679, 2009.

Cao, J.-J., Shen, Z.-X., Chow, J. C., Watson, J. G., Lee, S.-C., Tie, X.-X., Ho, K.-F., Wang, G.-H., and Han, Y.-M.: Winter and Summer PM2.5 Chemical Compositions in Fourteen Chinese Cities, J Air Waste Manage, 62, 1214-1226, 10.1080/10962247.2012.701193, 2012.

Chan, Y. C., Evans, M. J., He, P. Z., Holmes, C. D., Jaegle, L., Kasibhatla, P., Liu, X. Y., Sherwen, T., Thornton, J. A., Wang, X., Xie, Z. Q., Zhai, S. T., and

Alexander, B.: Heterogeneous Nitrate Production Mechanisms in Intense Haze Events in the North China Plain, Journal of Geophysical Research-Atmospheres, 126, 10.1029/2021jd034688, 2021.
Chang, Y. H., Zhang, Y. L., Tian, C. G., Zhang, S. C., Ma, X. Y., Cao, F., Liu, X. Y., Zhang, W. Q., Kuhn, T., and Lehmann, M. F.: Nitrogen isotope fractionation during gas-to-particle conversion of NOx to NO3- in the atmosphere - implications for isotope-based NOx source apportionment, Atmospheric Chemistry and Physics, 18, 11647-11661, 10.5194/acp-18-11647-2018, 2018.
Chen, H., Hu, R., Xie, P., Xing, X., Ling, L., Li, Z., Wang, F., Wang, Y., Liu, J., and Liu, W.: A hydroxyl radical detection system using gas expansion and fast gating laser-induced fluorescence techniques, J. Environ. Sci., 65, 190-200, 10.1016/j.jes.2017.03.012, 2018.
Chen, X., Walker, J. T., and Geron, C.: Chromatography related performance of the Monitor for AeRosols and GAses in ambient air (MARGA): laboratory and field-based evaluation, Atmos. Meas. Tech., 10, 3893-3908, 10.5194/amt-10-3893-2017, 2017.
Chen, X., Wang, H., and Lu, K.: Interpretation of NO3-N2O5 observation via steady state in high-aerosol air mass: the impact of equilibrium coefficient in ambient conditions, Atmospheric Chemistry and Physics, 22, 3525-3533, 10.5194/acp-22-3525-2022, 2022.
Chen, X. R., Wang, H. C., Liu, Y. H., Su, R., Wang, H. L., Lou, S. R., and Lu, K. D.: Spatial characteristics of the nighttime oxidation capacity in the Yangtze River Delta, China, Atmospheric Environment, 208, 150-157, 10.1016/j.atmosenv.2019.04.012, 2019.
Chen, X. R., Wang, H. C., Lu, K. D., Li, C. M., Zhai, T. Y., Tan, Z. F., Ma, X. F., Yang, X. P., Liu, Y. H., Chen, S. Y., Dong, H. B., Li, X., Wu, Z. J., Hu, M., Zeng, L. M., and Zhang, Y. H.: Field Determination of Nitrate Formation Pathway in Winter Beijing, Environmental Science & Technology, 54, 9243-9253, 10.1021/acs.est.0c00972, 2020.
Elshorbany, Y. F., Steil, B., Brühl, C., and Lelieveld, J.: Impact of HONO on global atmospheric chemistry calculated with an empirical parameterization in the EMAC model, ACP, 12, 9977-10000, 10.5194/acp-12-9977-2012, 2012.
Fountoukis, C. and Nenes, A.: ISORROPIA II: a computationally efficient thermodynamic equilibrium model for K+-Ca2+-Mg2+-Nh(4)(+)-Na+-SO42--NO3--Cl--H2O aerosols, Atmospheric Chemistry and Physics, 7, 4639-4659, 2007.
Goliff, W. S., Stockwell, W. R., and Lawson, C. V.: The regional atmospheric chemistry mechanism, version 2, Atmospheric Environment, 68, 174-185, 10.1016/j.atmosenv.2012.11.038, 2013.
Guo, L., Hu, Y., Hu, Q., Lin, J., Li, C., Chen, J., Li, L., and Fu, H.: Characteristics and chemical compositions of particulate matter collected at the selected metro stations of Shanghai, China, Science of the Total Environment, 496, 443-452,

10.1016/j.scitotenv.2014.07.055, 2014.
Hagler, G. S. W., Bergin, M. H., Salmon, L. G., Yu, J. Z., Wan, E. C. H., Zheng, M., Zeng, L. M., Kiang, C. S., Zhang, Y. H., Lau, A. K. H., and Schauer, J. J.: Source areas and chemical composition of fine particulate matter in the Pearl River Delta region of China, Atmos. Environ., 40, 3802-3815, 10.1016/j.atmosenv.2006.02.032, 2006.
Jiang, M., Lu, K., Su, R., Tan, Z., Wang, H., Li, L., Fu, Q., Zhai, C., Tan, Q., Yue, D., Chen, D., Wang, Z., Xie, S., Zeng, L., and Zhang, Y.: Ozone formation and key VOCs in typical Chinese city clusters, Chinese Sci Bull, 63, 1130-1141, 2018.
Kanaya, Y., Fukuda, M., Akimoto, H., Takegawa, N., Komazaki, Y., Yokouchi, Y., Koike, M., and Kondo, Y.: Urban photochemistry in central Tokyo: 2. Rates and regimes of oxidant (O-3+NO2) production, Journal of Geophysical Research-Atmospheres, 113, 10.1029/2007jd008671, 2008.
Li, H. Y., Zhang, Q., Zhang, Q., Chen, C. R., Wang, L. T., Wei, Z., Zhou, S., Parworth, C., Zheng, B., Canonaco, F., Prevot, A. S. H., Chen, P., Zhang, H. L., Wallington, T. J., and He, K. B.: Wintertime aerosol chemistry and haze evolution in an extremely polluted city of the North China Plain: significant contribution from coal and biomass combustion, Atmospheric Chemistry and Physics, 17, 4751-4768, 2017.
Liu, X., Gu, J., Li, Y., Cheng, Y., Qu, Y., Han, T., Wang, J., Tian, H., Chen, J., and Zhang, Y.: Increase of aerosol scattering by hygroscopic growth: Observation, modeling, and implications on visibility, Atmos. Res., 132-133, 91-101, https://doi.org/10.1016/j.atmosres.2013.04.007, 2013.
Lou, S., Tan, Z., Gan, G., Chen, J., Wang, H., Gao, Y., Huang, D., Huang, C., Li, X., Song, R., Wang, H., Wang, M., Wang, Q., Wu, Y., and Huang, C.: Observation based study on atmospheric oxidation capacity in Shanghai during late-autumn: Contribution from nitryl chloride, Atmospheric Environment, 271, 118902, https://doi.org/10.1016/j.atmosenv.2021.118902, 2022.
Lu, K. D., Hofzumahaus, A., Holland, F., Bohn, B., Brauers, T., Fuchs, H., Hu, M., Haseler, R., Kita, K., Kondo, Y., Li, X., Lou, S. R., Oebel, A., Shao, M., Zeng, L. M., Wahner, A., Zhu, T., Zhang, Y. H., and Rohrer, F.: Missing OH source in a suburban environment near Beijing: observed and modelled OH and HO2 concentrations in summer 2006, Atmospheric Chemistry and Physics, 13, 1057-1080, 10.5194/acp-13-1057-2013, 2013.
Lu, K. D., Rohrer, F., Holland, F., Fuchs, H., Bohn, B., Brauers, T., Chang, C. C., Haseler, R., Hu, M., Kita, K., Kondo, Y., Li, X., Lou, S. R., Nehr, S., Shao, M., Zeng, L. M., Wahner, A., Zhang, Y. H., and Hofzumahaus, A.: Observation and modelling of OH and HO2 concentrations in the Pearl River Delta 2006: a missing OH source in a VOC rich atmosphere, Atmospheric Chemistry and Physics, 12, 1541-1569, 10.5194/acp-12-1541-2012, 2012.
Ma, X. F., Tan, Z. F., Lu, K. D., Yang, X. P., Chen, X. R., Wang, H. C., Chen, S. Y., Fang, X., Li, S. L., Li, X., Liu, J. W., Liu, Y., Lou, S. R., Qiu, W. Y., Wang, H.

L., Zeng, L. M., and Zhang, Y. H.: OH and HO2 radical chemistry at a suburban site during the EXPLORE-YRD campaign in 2018, Atmospheric Chemistry and Physics, 22, 7005-7028, 2022.

Meng, Z. Y., Wu, L. Y., Xu, X. D., Xu, W. Y., Zhang, R. J., Jia, X. F., Liang, L. L., Miao, Y. C., Cheng, H. B., Xie, Y. L., He, J. J., and Zhong, J. T.: Changes in ammonia and its effects on PM2.5 chemical property in three winter seasons in Beijing, China, Science of the Total Environment, 749, 2020.

Ming, L., Jin, L., Li, J., Fu, P., Yang, W., Liu, D., Zhang, G., Wang, Z., and Li, X.: PM2.5 in the Yangtze River Delta, China: Chemical compositions, seasonal variations, and regional pollution events, Environmental Pollution, 223, 200-212, 10.1016/j.envpol.2017.01.013, 2017.

Phillips, G. J., Thieser, J., Tang, M. J., Sobanski, N., Schuster, G., Fachinger, J., Drewnick, F., Borrmann, S., Bingemer, H., Lelieveld, J., and Crowley, J. N.: Estimating N2O5 uptake coefficients using ambient measurements of NO3, N2O5, ClNO2 and particle-phase nitrate, Atmospheric Chemistry and Physics, 16, 13231-13249, 10.5194/acp-16-13231-2016, 2016.

Qin, Y., Li, J. Y., Gong, K. J., Wu, Z. J., Chen, M. D., Qin, M. M., Huang, L., and Hu, J. L.: Double high pollution events in the Yangtze River Delta from 2015 to 2019: Characteristics, trends, and meteorological situations, Science of the Total Environment, 792, 10.1016/j.scitotenv.2021.148349, 2021.

Qiu, X. H., Ying, Q., Wang, S. X., Duan, L., Zhao, J., Xing, J., Ding, D., Sun, Y. L., Liu, B. X., Shi, A. J., Yan, X., Xu, Q. C., and Hao, J. M.: Modeling the impact of heterogeneous reactions of chlorine on summertime nitrate formation in Beijing, China, Atmospheric Chemistry and Physics, 19, 6737-6747, 10.5194/acp-19-6737-2019, 2019.

Seinfeld, J. H. and Pandis, S. N.: Atmospheric chemistry and physics: from air pollution to climate change, Third;3rd;, Book, Whole, Wiley, Hoboken, New Jersey2016.

Shang, D. J., Peng, J. F., Guo, S., Wu, Z. J., and Hu, M.: Secondary aerosol formation in winter haze over the Beijing-Tianjin-Hebei Region, China, Front. Env. Sci. Eng., 15, 13, 10.1007/s11783-020-1326-x, 2021.

Shu, L., Wang, T. J., Xie, M., Li, M. M., Zhao, M., Zhang, M., and Zhao, X. Y.: Episode study of fine particle and ozone during the CAPUM-YRD over Yangtze River Delta of China: Characteristics and source attribution, Atmospheric Environment, 203, 87-101, 10.1016/j.atmosenv.2019.01.044, 2019.

Song, C. H. and Carmichael, G. R.: Gas-particle partitioning of nitric acid modulated by alkaline aerosol, Journal of Atmospheric Chemistry, 40, 1-22, 2001.

Staudt, S., Gord, J. R., Karimova, N. V., McDuffie, E. E., Brown, S. S., Gerber, R. B., Nathanson, G. M., and Bertram, T. H.: Sulfate and Carboxylate Suppress the Formation of ClNO2 at Atmospheric Interfaces, Acs Earth and Space Chemistry, 3, 1987-1997, 2019.

Sun, Y. L., Zhuang, G. S., Tang, A. H., Wang, Y., and An, Z. S.: Chemical

588 characteristics of PM2.5 and PM10 in haze-fog episodes in Beijing,
589 Environmental Science & Technology, 40, 3148-3155, 10.1021/es051533g,
590 2006.
591 Tan, Z., Wang, H., Lu, K., Dong, H., Liu, Y., Zeng, L., Hu, M., and Zhang, Y.: An
592 Observational Based Modeling of the Surface Layer Particulate Nitrate in the
593 North China Plain During Summertime, Journal of Geophysical Research:
594 Atmospheres, 126, e2021JD035623, https://doi.org/10.1029/2021JD035623,
595 2021.
596 Tan, Z. F., Lu, K. D., Dong, H. B., Hu, M., Li, X., Liu, Y. H., Lu, S. H., Shao, M., Su,
597 R., Wang, H. C., Wu, Y. S., Wahner, A., and Zhang, Y. H.: Explicit diagnosis of
598 the local ozone production rate and the ozone-NOx-VOC sensitivities, Science
599 Bulletin, 63, 1067-1076, 10.1016/j.scib.2018.07.001, 2018.
600 Tan, Z. F., Fuchs, H., Lu, K. D., Hofzumahaus, A., Bohn, B., Broch, S., Dong, H. B.,
601 Gomm, S., Haseler, R., He, L. Y., Holland, F., Li, X., Liu, Y., Lu, S. H., Rohrer,
602 F., Shao, M., Wang, B. L., Wang, M., Wu, Y. S., Zeng, L. M., Zhang, Y. S.,
603 Wahner, A., and Zhang, Y. H.: Radical chemistry at a rural site (Wangdu) in the
604 North China Plain: observation and model calculations of OH, HO2 and RO2
605 radicals, Atmospheric Chemistry and Physics, 17, 663-690, 10.5194/acp-17-663-
606 2017, 2017.
607 Tham, Y. J., Wang, Z., Li, Q., Wang, W., Wang, X., Lu, K., Ma, N., Yan, C.,
608 Kecorius, S., Wiedensohler, A., Zhang, Y., and Wang, T.: Heterogeneous N2O5
609 uptake coefficient and production yield of ClNO2 in polluted northern China:
610 roles of aerosol water content and chemical composition, Atmospheric
611 Chemistry and Physics, 18, 13155-13171, 10.5194/acp-18-13155-2018, 2018.
612 Wang, H., Lu, K., Chen, X., Zhu, Q., Chen, Q., Guo, S., Jiang, M., Li, X., Shang, D.,
613 Tan, Z., Wu, Y., Wu, Z., Zou, Q., Zheng, Y., Zeng, L., Zhu, T., Hu, M., and
614 Zhang, Y.: High N2O5 Concentrations Observed in Urban Beijing: Implications
615 of a Large Nitrate Formation Pathway, Environmental Science and Technology
616 Letters, 4, 416-420, 10.1021/acs.estlett.7b00341, 2017a.
617 Wang, H. C. and Lu, K. D.: Determination and Parameterization of the Heterogeneous
618 Uptake Coefficient of Dinitrogen Pentoxide (N2O5), Prog. Chem., 28, 917-933,
619 10.7536/pc151225, 2016.
620 Wang, H. C., Chen, J., and Lu, K. D.: Development of a portable cavity-enhanced
621 absorption spectrometer for the measurement of ambient NO3 and N2O5:
622 experimental setup, lab characterizations, and field applications in a polluted
623 urban environment, Atmos. Meas. Tech., 10, 1465-1479, 10.5194/amt-10-1465-
624 2017, 2017b.
625 Wang, H. C., Lu, K. D., Chen, X. R., Zhu, Q. D., Wu, Z. J., Wu, Y. S., and Sun, K.:
626 Fast particulate nitrate formation via N2O5 uptake aloft in winter in Beijing,
627 Atmospheric Chemistry and Physics, 18, 10483-10495, 10.5194/acp-18-10483-
628 2018, 2018a.
629 Wang, H. C., Chen, X. R., Lu, K. D., Hu, R. Z., Li, Z. Y., Wang, H. L., Ma, X. F.,

630 Yang, X. P., Chen, S. Y., Dong, H. B., Liu, Y., Fang, X., Zeng, L. M., Hu, M.,
631 and Zhang, Y. H.: NO3 and N2O5 chemistry at a suburban site during the
632 EXPLORE-YRD campaign in 2018, Atmospheric Environment, 224, 9,
633 10.1016/j.atmosenv.2019.117180, 2020a.
634 Wang, H. C., Chen, X. R., Lu, K. D., Tan, Z. F., Ma, X. F., Wu, Z. J., Li, X., Liu, Y.
635 H., Shang, D. J., Wu, Y. S., Zeng, L. M., Hu, M., Schmitt, S., Kiendler-Scharr,
636 A., Wahner, A., and Zhang, Y. H.: Wintertime N2O5 uptake coefficients over
637 the North China Plain, Science Bulletin, 65, 765-774,
638 10.1016/j.scib.2020.02.006, 2020b.
639 Wang, H. C., Lu, K. D., Guo, S., Wu, Z. J., Shang, D. J., Tan, Z. F., Wang, Y. J., Le
640 Breton, M., Lou, S. R., Tang, M. J., Wu, Y. S., Zhu, W. F., Zheng, J., Zeng, L.
641 M., Hallquist, M., Hu, M., and Zhang, Y. H.: Efficient N2O5 uptake and NO3
642 oxidation in the outflow of urban Beijing, Atmospheric Chemistry and Physics,
643 18, 9705-9721, 10.5194/acp-18-9705-2018, 2018b.
644 Wang, S. B., Wang, L. L., Fan, X. G., Wang, N., Ma, S. L., and Zhang, R. Q.:
645 Formation pathway of secondary inorganic aerosol and its influencing factors in
646 Northern China: Comparison between urban and rural sites, Science of the Total
647 Environment, 840, 2022.
648 Wang, X. F., Zhang, Y. P., Chen, H., Yang, X., Chen, J. M., and Geng, F. H.:
649 Particulate Nitrate Formation in a Highly Polluted Urban Area: A Case Study by
650 Single-Particle Mass Spectrometry in Shanghai, Environmental Science &
651 Technology, 43, 3061-3066, 2009.
652 Wang, Z., Wang, W. H., Tham, Y. J., Li, Q. Y., Wang, H., Wen, L., Wang, X. F., and
653 Wang, T.: Fast heterogeneous N2O5 uptake and ClNO2 production in power
654 plant and industrial plumes observed in the nocturnal residual layer over the
655 North China Plain, Atmospheric Chemistry and Physics, 17, 12361-12378,
656 10.5194/acp-17-12361-2017, 2017c.
657 Woodward-Massey, R., Slater, E. J., Alen, J., Ingham, T., Cryer, D. R., Stimpson, L.
658 M., Ye, C. X., Seakins, P. W., Whalley, L. K., and Heard, D. E.: Implementation
659 of a chemical background method for atmospheric OH measurements by laser-
660 induced fluorescence: characterisation and observations from the UK and China,
661 Atmos. Meas. Tech., 13, 3119-3146, 10.5194/amt-13-3119-2020, 2020.
662 Wu, S. P., Dai, L. H., Zhu, H., Zhang, N., Yan, J. P., Schwab, J. J., and Yuan, C. S.:
663 The impact of sea-salt aerosols on particulate inorganic nitrogen deposition in
664 the western Taiwan Strait region, China, Atmos. Res., 228, 68-76, 2019.
665 Xia, M., Peng, X., Wang, W., Yu, C., Sun, P., Li, Y., Liu, Y., Xu, Z., Wang, Z., Xu,
666 Z., Nie, W., Ding, A., and Wang, T.: Significant production of ClNO2 and
667 possible source of Cl-2 from N2O5 uptake at a suburban site in eastern China,
668 Atmospheric Chemistry and Physics, 20, 6147-6158, 10.5194/acp-20-6147-2020,
669 2020.
670 Xu, J. W., Huang, X., Wang, N., Li, Y. Y., and Ding, A. J.: Understanding ozone
671 pollution in the Yangtze River Delta of eastern China from the perspective of

672 diurnal cycles, Science of the Total Environment, 752,
673 10.1016/j.scitotenv.2020.141928, 2021.
674 Xue, H., Liu, G., Zhang, H., Hu, R., and Wang, X.: Similarities and differences in
675 PM10 and PM2.5 concentrations, chemical compositions and sources in Hefei
676 City, China, Chemosphere, 220, 760-765, 10.1016/j.chemosphere.2018.12.123,
677 2019.
678 Yang, X. P., Lu, K. D., Ma, X. F., Liu, Y. H., Wang, H. C., Hu, R. Z., Li, X., Lou, S.
679 R., Chen, S. Y., Dong, H. B., Wang, F. Y., Wang, Y. H., Zhang, G. X., Li, S. L.,
680 Yang, S. D., Yang, Y. M., Kuang, C. L., Tan, Z. F., Chen, X. R., Qiu, P. P.,
681 Zeng, L. M., Xie, P. H., and Zhang, Y. H.: Observations and modeling of OH
682 and HO2 radicals in Chengdu, China in summer 2019, Science of the Total
683 Environment, 772, 2021.
684 Yu, C., Wang, Z., Xia, M., Fu, X., Wang, W. H., Tham, Y. J., Chen, T. S., Zheng, P.
685 G., Li, H. Y., Shan, Y., Wang, X. F., Xue, L. K., Zhou, Y., Yue, D. L., Ou, Y.
686 B., Gao, J., Lu, K. D., Brown, S. S., Zhang, Y. H., and Wang, T.: Heterogeneous
687 N2O5 reactions on atmospheric aerosols at four Chinese sites: improving model
688 representation of uptake parameters, Atmospheric Chemistry and Physics, 20,
689 4367-4378, 10.5194/acp-20-4367-2020, 2020a.
690 Yu, C. A., Wang, Z., Ma, Q. X., Xue, L. K., George, C., and Wang, T.: Measurement
691 of heterogeneous uptake of NO2 on inorganic particles, sea water and urban
692 grime, J. Environ. Sci., 106, 124-135, 10.1016/j.jes.2021.01.018, 2021.
693 Yu, D., Tan, Z., Lu, K., Ma, X., Li, X., Chen, S., Zhu, B., Lin, L., Li, Y., Qiu, P.,
694 Yang, X., Liu, Y., Wang, H., He, L., Huang, X., and Zhang, Y.: An explicit
695 study of local ozone budget and NOx-VOCs sensitivity in Shenzhen China,
696 Atmospheric Environment, 224, 117304, 10.1016/j.atmosenv.2020.117304,
697 2020b.
698 Zhang, K., Xu, J. L., Huang, Q., Zhou, L., Fu, Q. Y., Duan, Y. S., and Xiu, G. L.:
699 Precursors and potential sources of ground-level ozone in suburban Shanghai,
700 Front. Env. Sci. Eng., 14, 10.1007/s11783-020-1271-8, 2020a.
701 Zhang, R., Han, Y. H., Shi, A. J., Sun, X. S., Yan, X., Huang, Y. H., and Wang, Y.:
702 Characteristics of ambient ammonia and its effects on particulate ammonium in
703 winter of urban Beijing, China, Environ Sci Pollut R, 28, 62828-62838, 2021.
704 Zhang, Y., Hong, Z., Chen, J., Xu, L., Hong, Y., Li, M., Hao, H., Chen, Y., Qiu, Y.,
705 Wu, X., Li, J.-R., Tong, L., and Xiao, H.: Impact of control measures and
706 typhoon weather on characteristics and formation of PM2.5 during the 2016 G20
707 summit in China, Atmospheric Environment, 224, 117312,
708 https://doi.org/10.1016/j.atmosenv.2020.117312, 2020b.
709 Zhang, Y., Tang, L., Yu, H., Wang, Z., Sun, Y., Qin, W., Chen, W., Chen, C., Ding,
710 A., Wu, J., Ge, S., Chen, C., and Zhou, H.-c.: Chemical composition, sources and
711 evolution processes of aerosol at an urban site in Yangtze River Delta, China
712 during wintertime, Atmospheric Environment, 123, 339-349,
713 10.1016/j.atmosenv.2015.08.017, 2015.

Zhang, Y., Tang, L., Croteau, P. L., Favez, O., Sun, Y., Canagaratna, M. R., Wang, Z., Couvidat, F., Albinet, A., Zhang, H., Sciare, J., Prevot, A. S. H., Jayne, J. T., and Worsnop, D. R.: Field characterization of the PM2.5 Aerosol Chemical Speciation Monitor: insights into the composition, sources, and processes of fine particles in eastern China, Atmospheric Chemistry and Physics, 17, 14501-14517, 10.5194/acp-17-14501-2017, 2017.

Zhang, Y. Y., Tang, A. H., Wang, C., Ma, X., Li, Y. Z., Xu, W., Xia, X. P., Zheng, A. H., Li, W. Q., Fang, Z. G., Zhao, X. F., Peng, X. L., Zhang, Y. P., Han, J., Zhang, L. J., Collett, J. L., and Liu, X. J.: PM (2.5) and water-soluble inorganic ion concentrations decreased faster in urban than rural areas in China, J. Environ. Sci., 122, 83-91, 2022.

Zhao, P. S., Dong, F., He, D., Zhao, X. J., Zhang, X. L., Zhang, W. Z., Yao, Q., and Liu, H. Y.: Characteristics of concentrations and chemical compositions for PM2.5 in the region of Beijing, Tianjin, and Hebei, China, Atmospheric Chemistry and Physics, 13, 4631-4644, 10.5194/acp-13-4631-2013, 2013.

Zhao, Z. Z., Sun, N., Zhou, W. L., Ma, S. S., Li, X. D., Li, M. L., Zhang, X., Tang, S. S., and Ye, Z. L.: Chemical Compositions in Winter PM2.5 in Changzhou of the Yangtze River Delta Region, China: Characteristics and Atmospheric Responses Along With the Different Pollution Levels, Front Env Sci-Switz, 10, 2022.

Zheng, G. J., Duan, F. K., Su, H., Ma, Y. L., Cheng, Y., Zheng, B., Zhang, Q., Huang, T., Kimoto, T., Chang, D., Poschl, U., Cheng, Y. F., and He, K. B.: Exploring the severe winter haze in Beijing: the impact of synoptic weather, regional transport and heterogeneous reactions, Atmospheric Chemistry and Physics, 15, 2969-2983, 2015.